

**3. Results of Flight Scientific Programmes, Research and Observation
Realized (Implemented) in 2013-2015**

**3.1 A simple technique has been developed for estimations of the soft
X-ray class of far-side solar flares observed with STEREO spacecraft**

It is an example of how a parasitic effect can be used to obtain quite useful information.

Around the peaks of substantial flares of the C class and above, a bright spurious nearly horizontal saturation streaks (B-streaks) corresponding to the brightest parts of the flare sources appear in the STEREO/EUVI 195 Å images.

These streaks are a consequence of the so-called blooming, *i.e.*, saturation of CCD cells, imaging the brightest flare source, and spilling of excessive electrons from these cells along CCD columns.

The maximum length of these B-streaks can be used to solve the problem of evaluating the soft X-ray flux and class of far-side flares that are registered with the twin STEREO spacecraft, but are invisible from Earth (Fig.1).

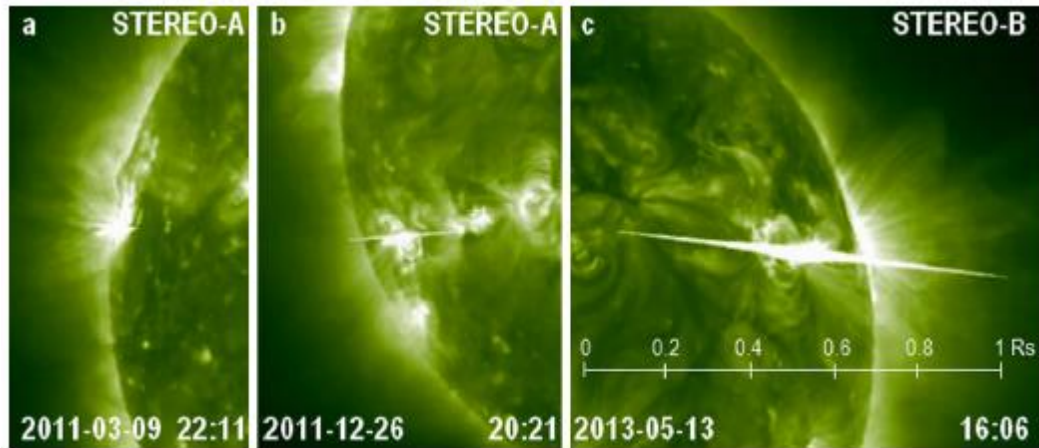


Fig.1.The STEREO/EUVI 195 Å B-streaks typical of C-,M-, and X-class flares. The spatial scale shown in panel (c) is the same for all of the three images.

For this purpose, from data on about 350 flares observed from January 2007 to July both with GOES and STEREO, an empirical relation that correlates the GOES 1 – 8 Å peak flux and the B-streak relative length (L/R_s) was established. This allows to estimate the soft X-ray classes of behind-the-limb flares (Figure 2).

It is found that in the short-term compact flares a single, thin, and relatively long B-streak is usually observed. In contrast, the long-duration (LDE) flares produce relatively short, but thick B-streaks with two or more blooming elements. It is demonstrated that B-streaks in several consecutive EUVI images can be used to reconstruct a probable time history of strong far-side flares.

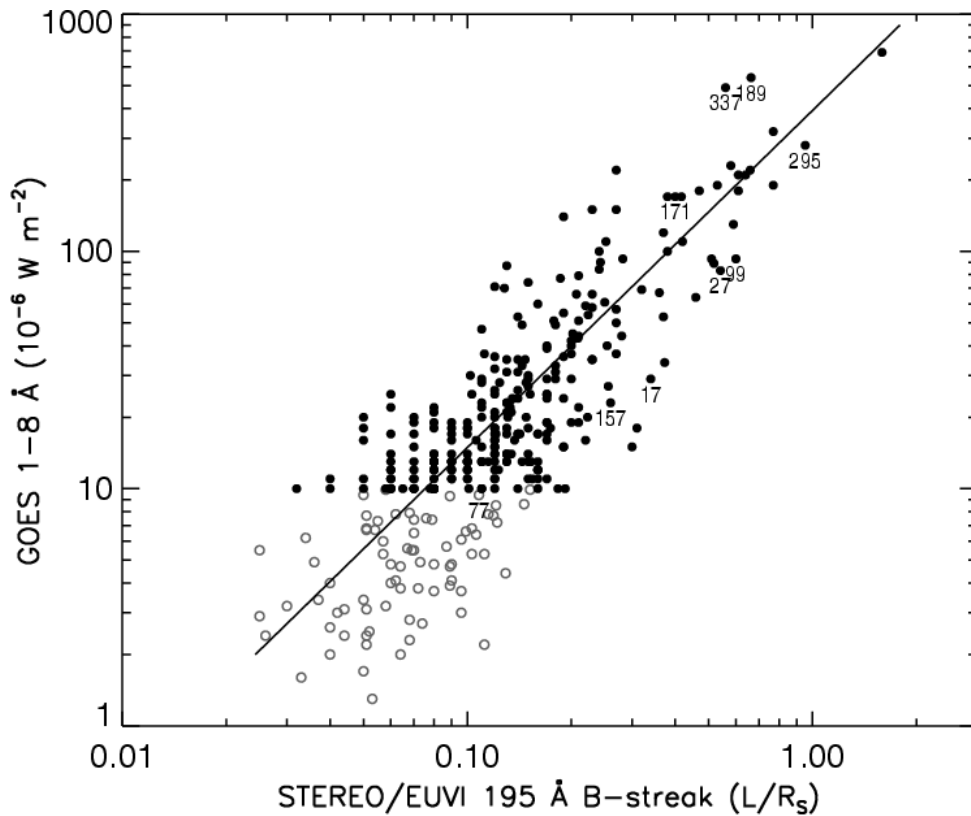


Fig.2. Scatter plot of the relative lengths of the STEREO/EUVI B-streaks versus the GOES 1 – 8 Å fluxes. The gray open circles denote C-class flares, and the black filled circles denote \geq M1-class flares.

The established dependence allowed to estimate the soft X-ray class of approximately 65 strong far-side flares with $L/R_s > 0.2$ (i.e. with importance $> M3.0$) observed by STEREO for the same years. According to these estimations, the most powerful flare of the solar cycle 24 occurred on 20 September 2012 in the active region with coordinates S15E156 and had the longest saturation streak $L/R_s \approx 2.38$. Its estimated soft X-ray class reached the X13 level. The proposed simple method gives the results which are consistent with estimations of Nitta *et al.* (*Solar Phys.* **288**, 241, 2013) that are based on the calculations of the EUVI full-disk digital number output.

Reference

Chertok I.M., Belov A.V., Grechnev V.V. A Simple Way to Estimate the Soft X-ray Class of Far-Side Solar Flares Observed with STEREO/EUVI. *Solar Phys.* Volume 290, Issue 7, pp. 1947-1961, 2015. DOI: 10.1007/s11207-015-0738-4. <http://arxiv.org/pdf/1505.01649v2.pdf>

3.2 Anomalous Positions of the Plasmapause and Ionospheric Trough as Inferred from DEMETER Data

A study was carried out to examine a specific pattern of the subauroral ionosphere characterized by anomalous positions of the plasmapause, equatorial boundary of the mid-latitude (main) ionospheric trough, and light-ion trough under quiet solar and geophysical conditions near the magnetospheric shell with the McIlwain parameter $L=3$ (Table 1).

The anomaly was identified using the data of active experiments with the SURA heating facility on October 2, 2007, which were conducted as part of the SURA–International Space Station (SURA–ISS) program in the framework of the DEMETER satellite mission. Joint analysis of the DEMETER and ISS orbital data together with the results of complex ground-based measurements shows that the revealed effect characteristic of the pre-midnight sector North of the Moscow–SURA satellite path is not local. It is observed in a vast territory extending from the West to the East (Table 1) along the same L-shell from at least Sweden to Kamchatka. The conclusions based on the DEMETER data (Fig.1) are supported by the analysis of meridional distributions of the F2 peak plasma frequencies provided by GPS radio probing (Fig.2) of the ionosphere. Comparison of these results with the model latitudinal–longitudinal and meridional distributions of the F2 peak plasma density provided by IRI-2007 and SMI (Russian Standard Model Ionosphere) shows that the model predictions are at odds with the empirical data (Fig.1 and 2).

Table 1.

McIlwain L -parameter calculated for a number of orbits of the DEMETER satellite

Orbit no. (660 km)	Latitude, deg	Longitude, deg	Height (at equator), km	McIlwain L -parameter
17363	59.00	110.0	13137	3.06
17364	58.36	86.56	13185	3.07
17365	57.36	62.63	12388	2.94
17366	56.36	38.68	12215	2.92
17367	55.63	14.54	12317	2.93

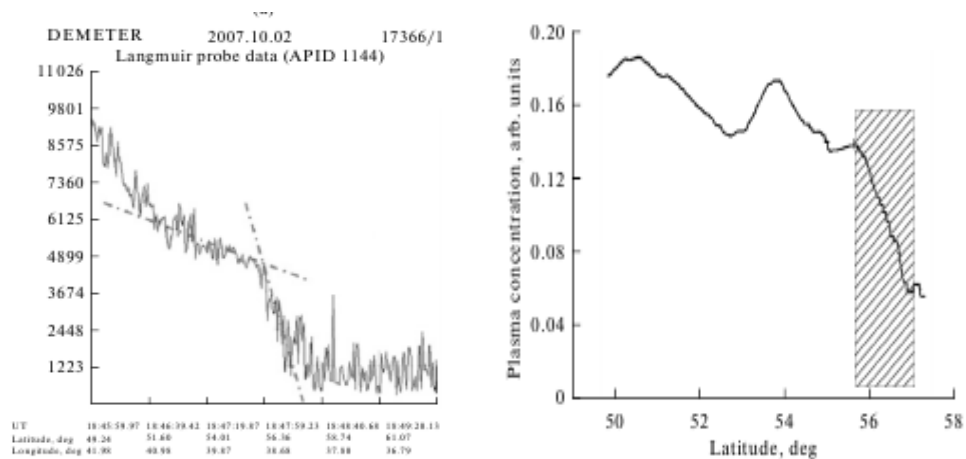


Fig.1. (Left) Plasma concentrations vs. time along the orbit of the DEMETER satellite in the region of the experiment.

Fig.2. (Right) Latitude dependence of the F2 peak plasma density on October 2, 2007 (GPS 14 satellite). The segment to the North of the IZMIRAN–SURA latitude is indicated.

Reference

Yu. Ya. Ruzhin, M. Parrot, V. M. Smirnov, and V. Kh. Depuev. The Anomaly of Plasmopause and Ionospheric Trough Positions from DEMETER Data. ISSN 001667932, Geomagnetism and Aeronomy, 2014, Vol. 54, No. 6, pp. 763–772.

3.3 The disturbances in the ionosphere-plasmasphere parameters recorded during the geomagnetic storm of 26 September 2011 were analyzed using the Global Consistent Model Thermosphere-

Ionosphere-Protonosphere (GCM TIP) and data from the receiver network of the GLONASS/GPS global satellite navigation systems

The analysis revealed a global response of the total and plasmaspheric electron content to the geomagnetic storm. Variations in the relative contribution of the plasmaspheric electron content (PEC, from 700 to 20200 km) to the total electron content (TEC) during the storm main phase were studied for the first time. In the main phase of the storm, the mid-latitude ionosphere is more variable than the plasmasphere and makes a major contribution to the TEC disturbance represented in Fig.1 (Klimenko et al., 2015).

It is shown that at the mid and equatorial latitudes, there form regions, in which the contribution of PEC to TEC increases by 20–25%. This suggests that the plasmasphere/protonosphere conditions must be taken into account when solving positioning problems with the use of up-to-date satellite navigation systems.

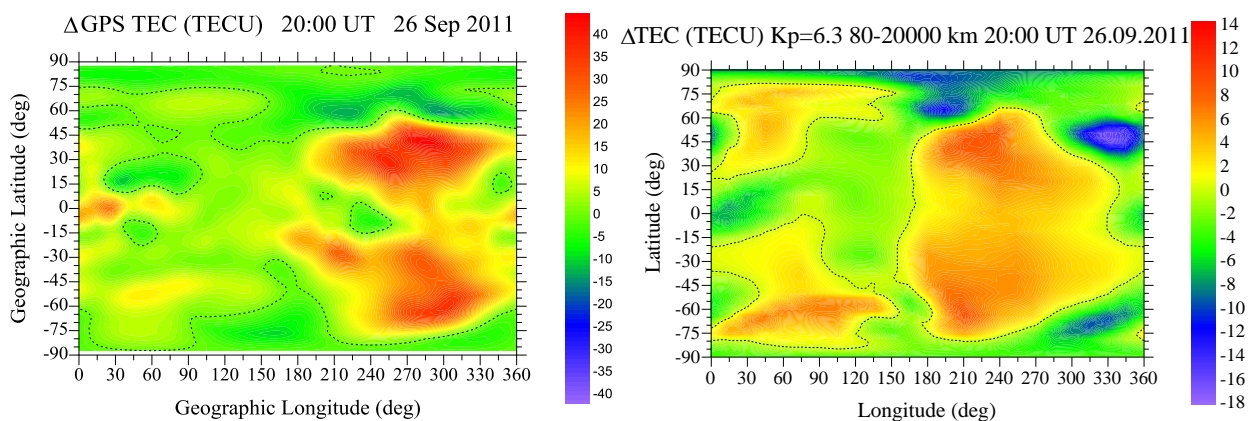


Fig.1. Global maps of TEC disturbances in the main phase of geomagnetic storm on 26 Sept. at 20:00 UT based on the Global Positioning System (GPS) data (left) and on model calculations (right).

Positive disturbances of electron density were detected for the first time in the recovery phase of geomagnetic storm in the mid-latitude ionospheric F-region as a result of increase in the $n(O)/n(N_2)$ ratio in the daytime hours. At night,

negative effects are formed, because the plasma tubes depleted in the storm main phase remain incompletely filled in spite of the decrease in $n(N_2)$.

Reference

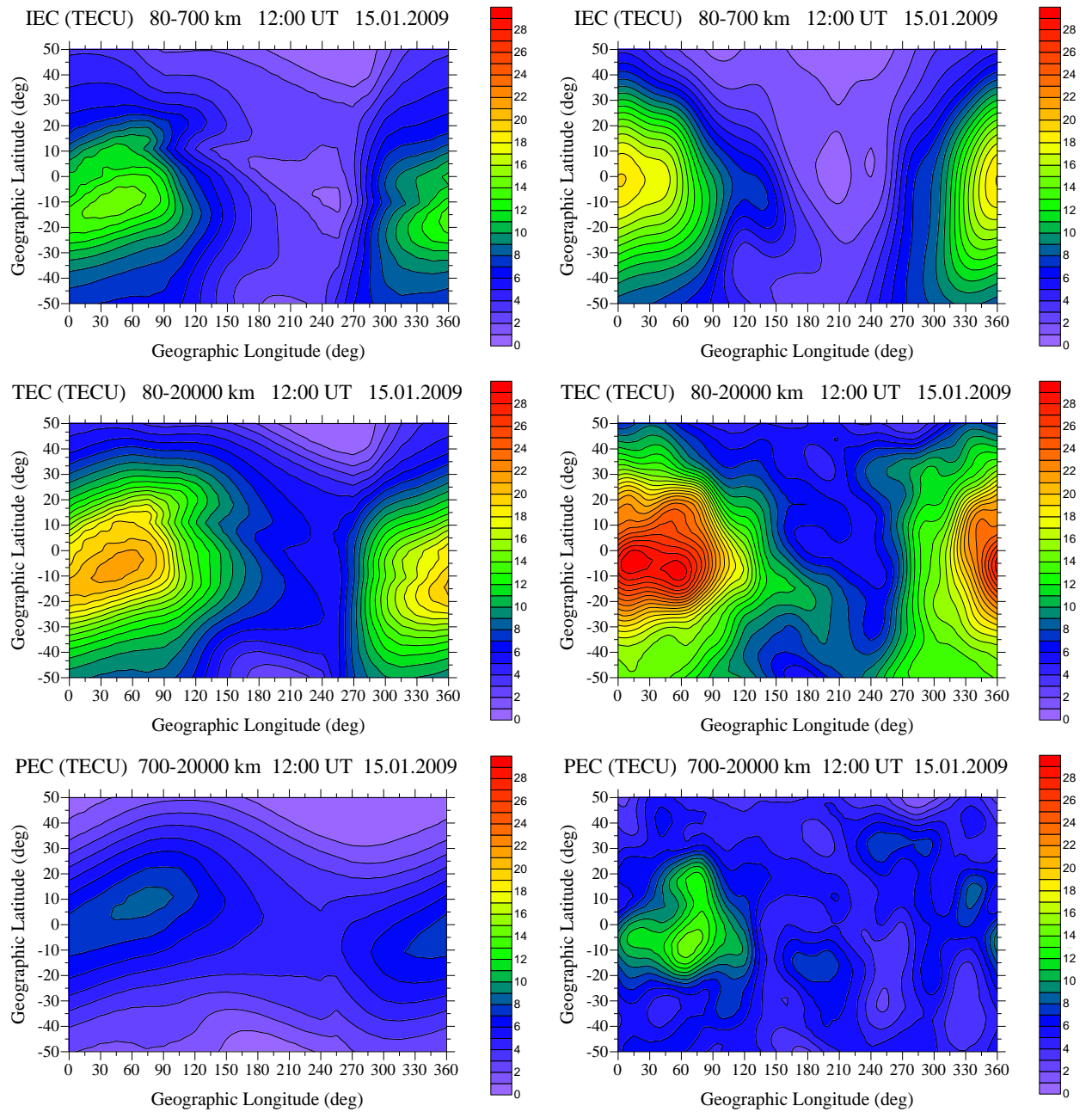
Klimenko M.V., Klimenko V.V., Bessarab F.S., Ratovsky K.G., Zakharenkova I.E., Nosikov I.A., Stepanov S.E., Kotova D.S., Vorob'yev V.G., Yagodkina O.I. The effect of the geomagnetic storms of 26 Sept. 2011 on the ionosphere and on HF radio propagation. I. Ionospheric effects. *Geomagn. and Aeron.*, 2015, v. 55, No. 5, pp.769-789.

3.4 The study of contribution of the plasmasphere to the total electron content in winter 2009 (SA minimum)

Contribution of the plasmasphere to the total electron content in winter 2009 (SA minimum) was studied at all latitudes and longitudes both on the basis of model calculations and on the basis of ground and satellite (GPS, COSMIC) observations (see Fig.1).

As a result of the study, Klimenko et al. (2015a) arrived at the following conclusions: (1) the maximum contribution of the plasmasphere to TEC (up to 85%) is observed at night in the vicinity of the equator, where it exceeds the contribution of the ionosphere; and (2) the daytime contribution of the plasmasphere to TEC does not exceed 40%, which agrees with the results of earlier studies (Balan et al., 2002). Thus, the ionospheric electron content (from the Earth surface up to the height of 700 km) cannot be considered the only significant parameter when calculating TEC, since in some regions and periods of

time, particularly, at the minimum of solar and geomagnetic activity, both the ionosphere and the plasmasphere contribute significantly to TEC.



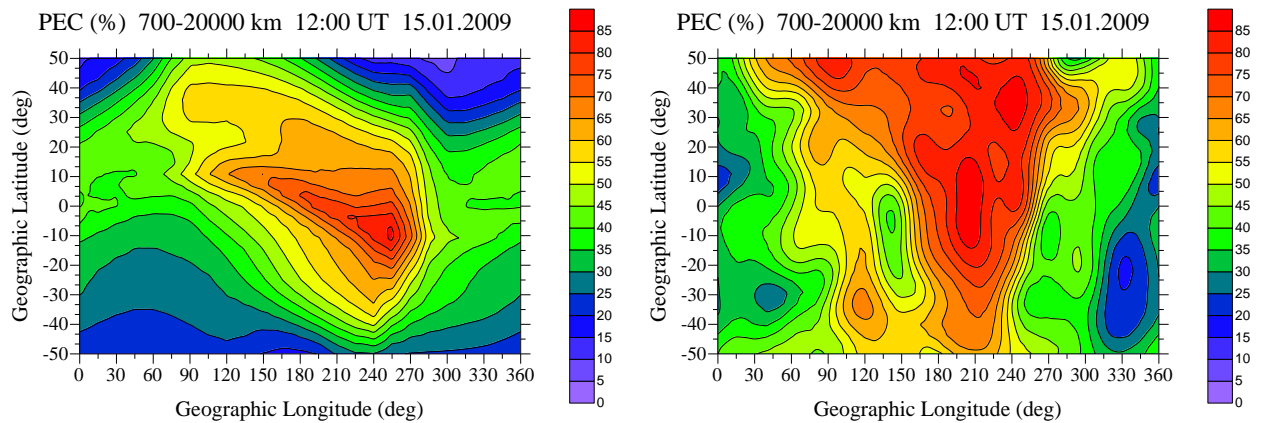


Fig.1. From top to bottom: maps of *IEC*, *TEC*, *PEC* in TECU and *PEC* in %. Left panel – GCM TIP results, right panel – *TEC* observation data from COSMIC and *TEC* from IONEX maps.

Reference

Klimenko M.V., Klimenko V.V., Zakharenkova I.E., Cherniak Iu.V. The global morphology of the plasmaspheric electron content during Northern winter 2009 based on GPS/COSMIC observation and GSM TIP model results. *Advances in Space Research*, 2015a, V. 55 (8), P. 2077-2085, doi:10.1016/j.asr.2014.06.027.

3.5 Concurrent observations on board GOCE and TerraSAR satellites

Concurrent observations carried out on board two Low-Earth-Orbit satellite missions were analyzed: the GOCE satellite with unprecedented low orbit of 250 km (Gravity field and steady-state Ocean Circulation Explorer) and the TerraSAR-X satellite with the orbit altitude of 515 km (see Fig.1).

The science payloads of both satellites have no instruments for ionospheric research, but they include a dual-frequency GPS receiver. GPS measurements from the POD (Precise Orbit Determination) GPS antenna onboard these satellites can be used to determine the total electron content in the topside ionosphere-plasmasphere system under different conditions. The results obtained from these missions are presented for the first time. The comparison was done for the June

and December solstice conditions at low and moderate solar activity and quiet geomagnetic field. We obtained quantitative estimates of electron content and its percentage contribution to the ground-based GPS TEC in the topside ionosphere/plasmasphere at altitudes of 250-500 km and above 500 km. Similar features and differences in the electron content distribution on a global scale were discussed. Particularities of the Weddell Sea Anomaly and Equatorial Ionization Anomaly are evident in the topside TEC derived from GOCE GPS data. The presence of the Weddell Sea Anomaly in TEC in the local early morning was reported.

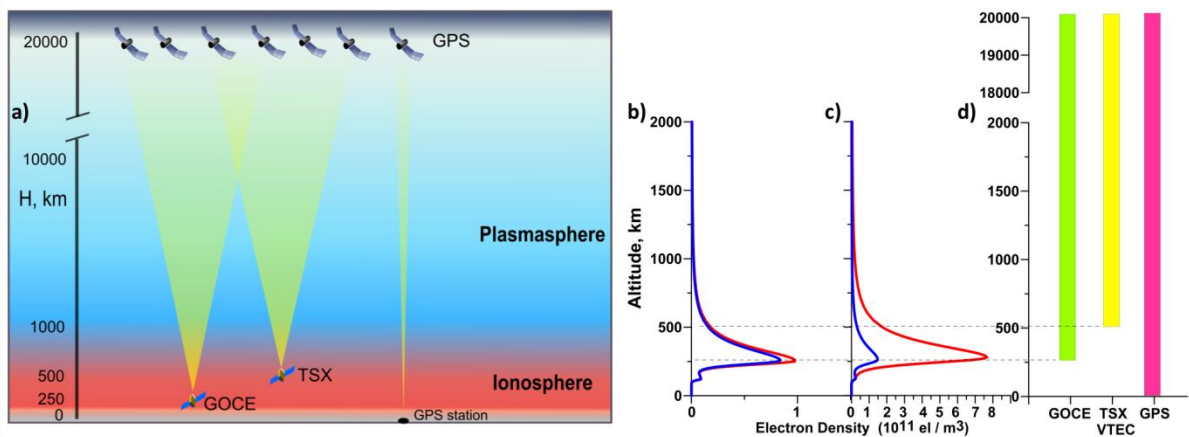


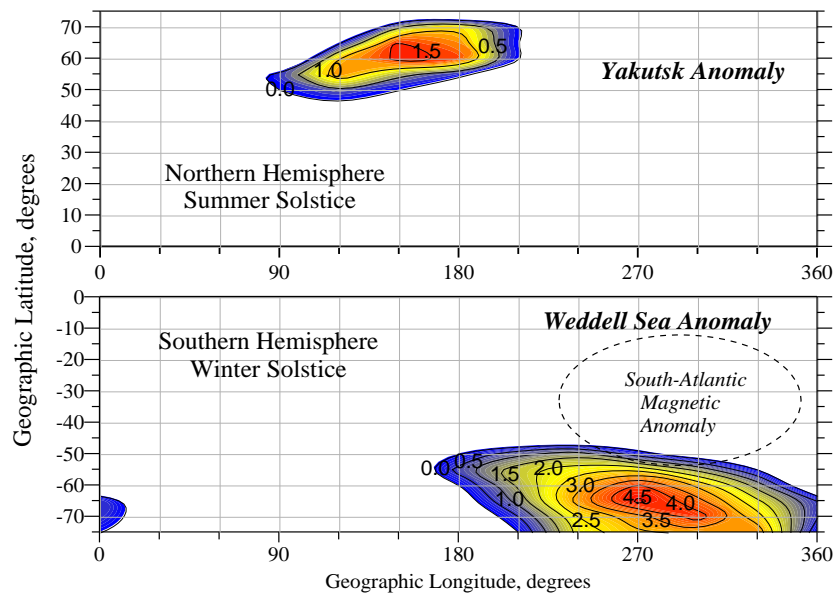
Fig.1. (a) Schematic view of the instrument configuration; samples of the ionospheric electron density profiles derived from NeQuick model for the conditions of 15 June 2010 at 06 LT (blue line) and 18 LT (red line) at (b) mid-latitude and (c) equatorial points with coordinates (40°S, 15°E) and (0°S, 15°E) correspondingly; (d) altitude ranges, which contributed to VTEC determination for each instrument. The dashed line shows the GOCE and TSX orbital altitude.

Reference

Zakharenkova, I., Cherniak, I. (2015). How can GOCE and TerraSAR-X contribute to the topside ionosphere and plasmasphere research? *Sp. Weather* 13, 271–285. doi:10.1002/2015SW001162.

3.6 Description of the electron-density variations at Weddell Sea and Yakutsk Anomalies

The unique bank of data obtained from the Intercosmos-19 and COSMIC satellites and the GPS global receiver network were used to verify the description of the electron-density longitudinal variations at subauroral latitudes (in particular, the Weddell Sea and Yakutsk Anomalies) based on GCM TIP and IRI (International Reference Ionosphere) calculations. For the first time, using IK-19 satellite data and GCM TIP and IRI models, Klimenko et al. (2015b) identified the formation regions of the Weddell Sea (WSA) and Yakutsk (YA) Anomalies, in which $foF2$ values in the local summer were greater at night than in the daytime (Fig.1).



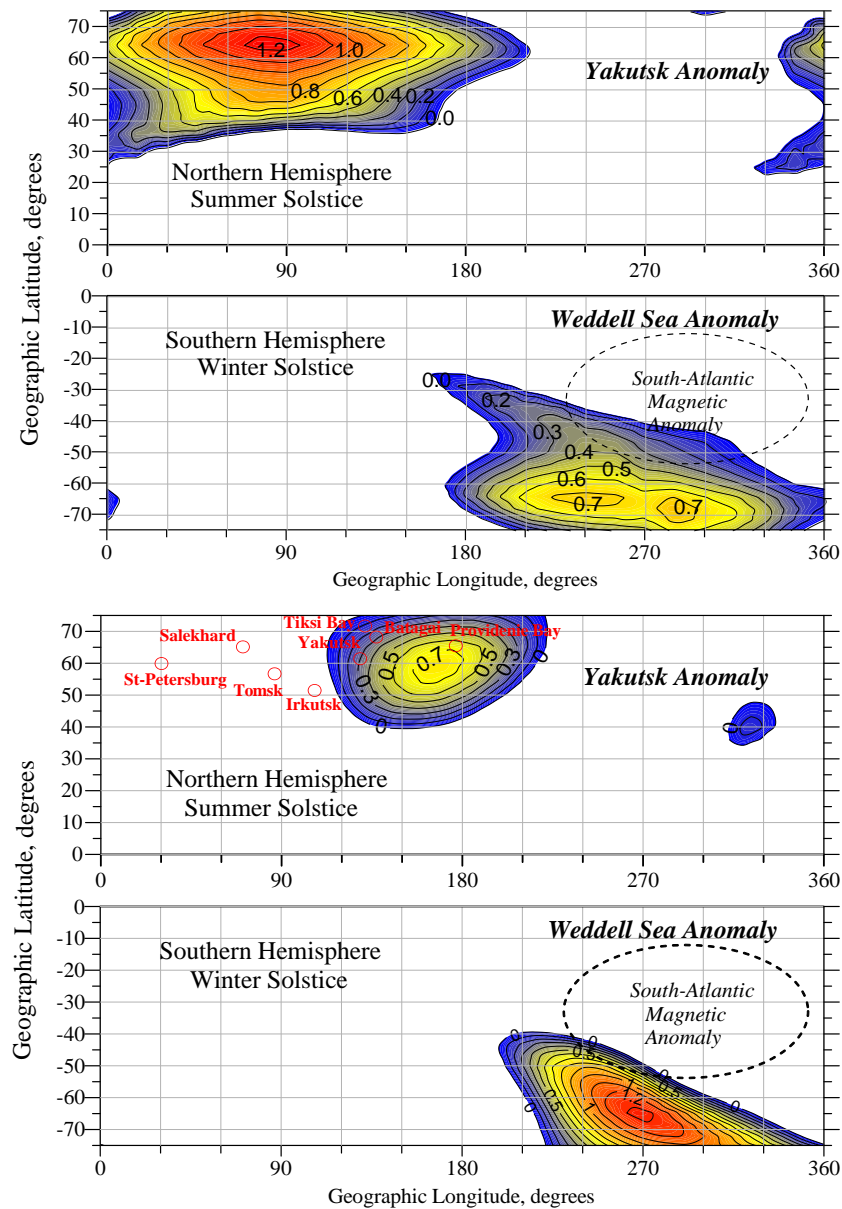


Fig.1. The maps of positive difference between the midnight and midday values of $foF2$ for WSA and YA. Top – IK-19 data; middle – GCM TIP results; bottom – IRI results.

Effects of the Weddell Sea Anomaly, Yakutsk Anomaly, and longitudinal structure of the main ionospheric trough (light ion trough) were revealed in the upper ionosphere, ionospheric and plasmaspheric total electron content. The plasmasphere does not have significant effect on the Weddell Sea and Yakutsk ionospheric anomalies, which are formed in the outer ionosphere earlier than in the $F2$ layer. It is shown that the main contribution to ground-based observations of the Weddell Sea anomaly in the total electron content comes from the heights of 250-500 km. Figure 2 shows that, in spite the presence of solar ionization over

the WSA and YA regions in the daytime and its absence at night, the nighttime values of $foF2$ are greater than the daytime ones because of (1) the horizontal plasma transport due to electromagnetic drift; (2) vertical plasma transport along the geomagnetic field lines due to the effect of the meridional component of the thermospheric wind; and (3) distribution of neutral constituents of the thermosphere. Klimenko et al. (2015c) reported differences between the subauroral anomalies (WSA и YA) and the mid-latitude summer sunset anomaly in $foF2$.

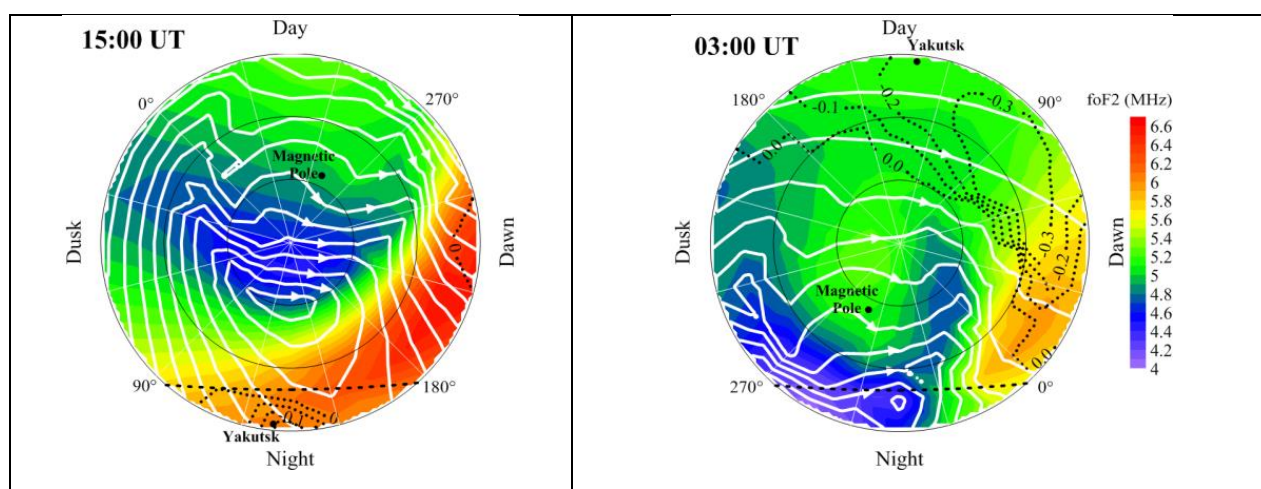


Fig.2. A scheme of formation of the Yakutsk Anomaly according to GCM TIP. The horizontal electromagnetic drift is shown with white lines; the arrows denote the direction of plasma transport.

Reference

1. Klimenko M.V., Klimenko V.V., Karpachev A.T., Ratovsky K.G., Stepanov A.E. Spatial features of Weddell Sea and Yakutsk Anomalies in $foF2$ diurnal variations during high solar activity periods: Interkosmos-19 satellite and ground-based ionosonde observations, IRI reproduction and GSM TIP model simulation. *Advances in Space Research*, 2015b, V. 55 (8), P. 2020-2032, doi:10.1016/j.asr.2014.12.032.
2. Klimenko M.V., Klimenko V.V., Ratovsky K.G., Zakharenkova I.E., Yasyukevich Yu.V., Korenkova N.A., Cherniak Iu.V., Mylnikova A.A. Mid-latitude Summer Evening Anomaly (MSEA) in F2 layer electron density and

Total Electron Content at solar minimum. *Advances in Space Research*, 2015c, V. 56(9), P. 1951-1960, doi:10.1016/j.asr.2015.07.019.

3.7 Compensation of the UHF radar error

Compensation of the UHF radar error was investigated depending on the parameters of radio propagation medium (model ionosphere). The study inferred the following conclusions: (1) the use of real-time data on f_oF2 and TEC from the neighboring stations for refining the model ionosphere improves the accuracy of positioning of the object by radars; (2) the procedure of real-time refinement of the model ionosphere is more efficient under quiet conditions than during geomagnetic disturbances; and (3) measurements of the slant total electron content can be used to reconstruct f_oF2 in the regions where vertical sounding stations are absent.

Reference

Ovodenko V.B., Trekin V.V., Korenkova N.A., Klimenko M.V. Investigating range error compensation in UHF radar through IRI-2007 real-time updating: Preliminary results. *Advances in Space Research*, 2015, V.56 (5), P. 900-906, doi:10.1016/j.asr.2015.05.017.

3.8. Disturbances in electron density during sudden stratospheric warming events

It is shown that the negative disturbances in electron density and total electron content at the auroral latitudes during sudden stratospheric warming events are due to the reduction of the O/N₂ ratio as a result of heating of the upper thermosphere. The disturbances in the total electron content observed during

sudden stratospheric warming events can be reproduced by specifying an additional electrical potential in the GCM TIP model (see Fig.1).

Thus, the changes in the zonal electric field (vertical plasma drift) are the key mechanism of the low-latitude ionosphere response to sudden stratospheric warming. However, it still remains unclear what is the mechanism of generation of such zonal electric fields at low latitudes during the sudden stratospheric warming events.

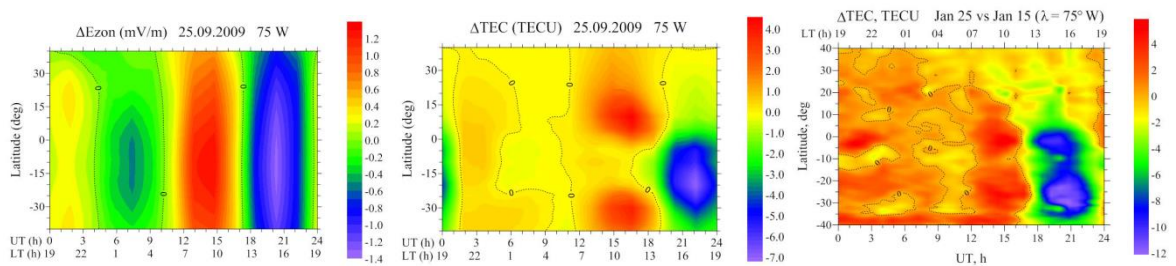


Fig.1. Diurnal variation of disturbances in the zonal electric field (left) and TEC (middle) at different latitudes at the longitude of 75°W on 25 January as calculated within the GCM TIP model. GPS observations of TEC are shown on the right.

Reference

Klimenko M. V., Klimenko V. V., Bessarab F. S., Korenkov Yu. N., Liu H., Goncharenko L. P., Tolstikov M. V. Study of the thermospheric and ionospheric response to the 2009 sudden stratospheric warming using TIME-GCM and GSM TIP models – first results. *J. Geophys. Res. Space Physics*, 2015d, V. 120, doi:10.1002/2014JA020861.

3.9. Fluctuations of GPS/GLONASS signals and auroral activity

We present results on the GNSS signal phase fluctuations occurrence during the geomagnetic storm of October 2, 2013 (Fig.1). We used the rate of TEC (ROT, in the unit of TECU/min, $1 \text{ TECU} = 10^{16} \text{ electron/m}^2$) at 1 min interval as a measure of fluctuations activity and index ROTI (standard deviation of ROT) as a measure of

fluctuation intensity. The data of GPS/GLONASS stations spaced in latitudinal range of 67-50 degrees along longitude of 20 degrees were involved in this analysis. The magnetograms of the IMAGE network, Lovozero, Sodankyla magnetometers were also used as an indicator of auroral activity.

For the October 2, 2013 geomagnetic storm the intense TEC fluctuations were observed at auroral and subauroral ionosphere. During intervals of the maximal auroral activity the intense phase fluctuations were registered even at the midlatitude station Kaliningrad. We reveal good agreement between temporal development of substorm activity and intensity of the TEC fluctuations. The highest correlation of GPS data fluctuations and optical and magnetic disturbances was achieved during this storm. The TEC fluctuations intensity during magnetic bay decreased from north to south. The images of spatial distribution of TEC fluctuations intensity (index ROTI) in CGL and MLT coordinates were constructed using daily GPS measurements from 130-150 selected stations. These images depict the irregularities oval, which was comparing with the auroral oval model (Fig.2). The auroral and irregularities ovals shifted equatorward during this storm. The analysis reveals that the high latitude phase fluctuations of GPS signals is very sensitive to changes of auroral activity and can be used as an indicator of space weather conditions.

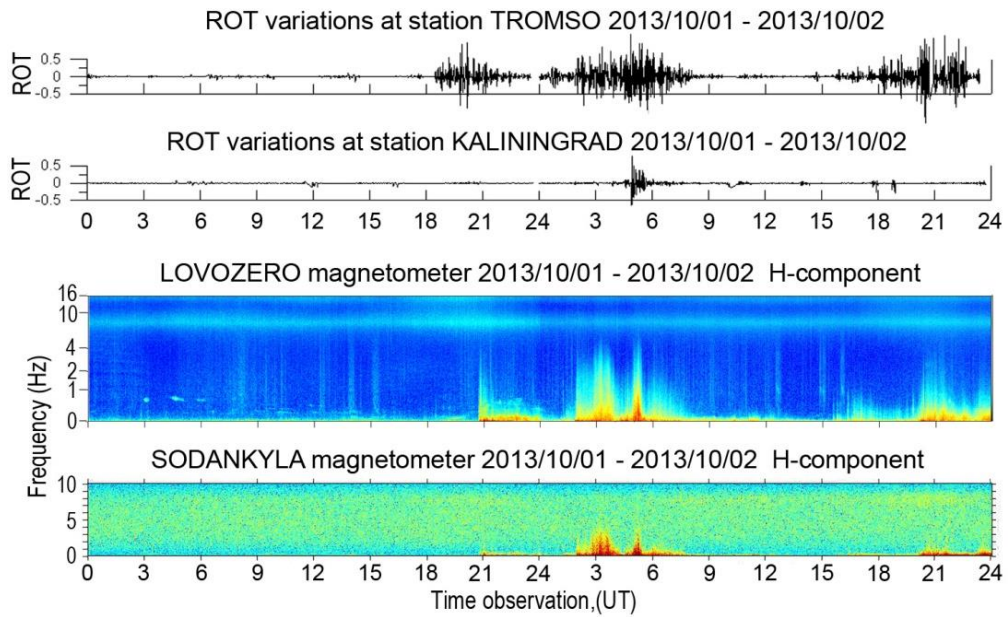


Fig.1. Occurrence of TEC fluctuations (index ROT) at auroral Tromso and midlatitude Kalinigrad stations and keograms at the stations Lovozero and Sodaynkyula for 1-2 October 2013.

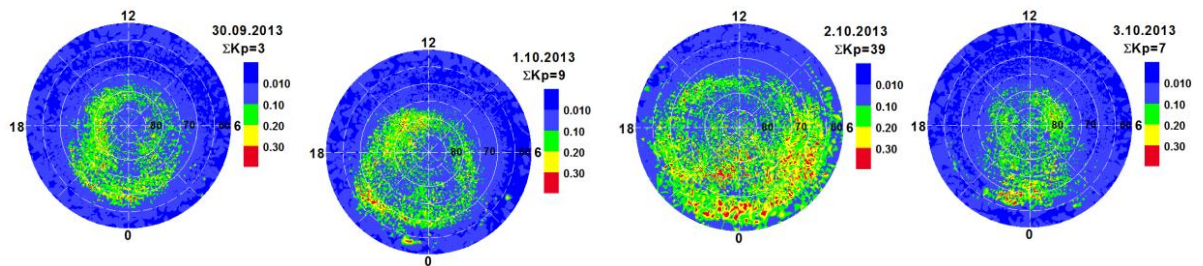


Fig.2. Daily dynamics of the irregularity oval in dependance on a geomagnetic activity from 30.09.2013 to 03.10.2013.

Reference

Shagimuratov I., Chernouss S., Cherniak Iu., Efishov I., Filatov M.2, Tepenitsyna N., Phase fluctuations of GPS signals and irregularities in the high latitude ionosphere during geomagnetic storm/ Sun and Geosphere, 2015, number11/12, p. 101-108.